Surface Science 627 (2014) 34–41

Contents lists available at ScienceDirect

Surface Science

journal homepage: www.elsevier.com/locate/susc

Ti adatom diffusion on TiN(001): Ab initio and classical molecular dynamics simulations

D.G. Sangiovanni [a,*], D. Edström [a], L. Hultman [a], I. Petrov [a,b,c,d], J.E. Greene [a,b,c,d], V. Chirita [a]

[a] Department of Physics, Chemistry and Biology (IFM), Linköping University, SE-58183 Linköping, Sweden
[b] Department of Materials Science, University of Illinois, Urbana, IL 61801, USA
[c] Department of Physics, University of Illinois, Urbana, IL 61801, USA
[d] Frederick Seitz Materials Research Laboratory, University of Illinois, Urbana, IL 61801, USA

ARTICLE INFO

Article history:
Received 14 February 2014
Accepted 8 April 2014
Available online 16 April 2014

Keywords:
Surface diffusion
Nitrides
Molecular dynamics simulations
Density functional theory

ABSTRACT

Ab initio and classical molecular dynamics (AIMD and CMD) simulations reveal that Ti adatoms on TiN(001) surfaces migrate between neighboring fourfold hollow sites primarily along in-plane <100> channels. <100> and <110> single jumps, as well as <100> double jump rates, obtained directly from MD runs as a function of temperature, are used to determine diffusion activation energies E_a, and attempt frequencies A, for the three preferred Ti adatom migration pathways on TiN(001). From transition rates $A\exp[-E_a/(k_BT)]$, we determine adatom surface distribution probabilities as a function of time, which are used to calculate adatom diffusion coefficients $D_s(T)$. AIMD and CMD predictions are consistent and complementary. Using CMD, we investigate the effect on the adatom jump rate of varying the phonon wavelength degrees of freedom by progressively increasing the supercell size. We find that long-wavelength phonons significantly contribute to increasing adatom mobilities at temperatures ≤600 K, but not at higher temperatures. Finally, by directly tracking the Ti adatom mean-square displacement during CMD runs, we find that Ti adatom jumps are highly correlated on TiN(001), an effect that yields lower D_s values (D_s^{corr}) than those estimated from uncorrelated transition probabilities. The temperature-dependent diffusion coefficient is $D_s^{corr}(T) = (4.5 \times 10^{-4}\ cm^2\ s^{-1}) \exp[-0.55\ eV/(k_BT)]$.

1. Introduction

Transition-metal (TM) nitrides exhibit excellent physical and mechanical properties, including high hardness [1,2] and toughness [3], chemical inertness, and good thermal stability and electrical conductivity [4]. Thus, they are employed in a wide variety of applications ranging from wear-resistant protective coatings on cutting tools and engine components [5,6] to diffusion barriers in electronic devices [7–11]. The properties and performance of TM nitrides layers ultimately depend on their nanostructure. During thin-film deposition, nanostructural and surface morphological evolution are largely controlled by the dynamics of adatom surface migration which, in turn, determine nucleation kinetics and film growth modes. A deeper understanding of these processes may allow better control of growth dynamics, and thus the ability to tailor film properties to specific requirements.

Very little is known about either the mechanisms or the kinetics of mass transport in TM nitride systems [12–14]. For TiN, the most studied and best characterized TM nitride [15], differences in reported bulk diffusion coefficients range over several orders of magnitude [14,16,17]. Moreover, surface mass transport properties lack experimental verification. This is due to the fact that even advanced atomic-scale experimental techniques, such as scanning tunneling microscopy [18–20] and low-energy electron microscopy [21–23], which provide important information regarding surface and nanostructure evolution, cannot provide detailed atomistic dynamics and kinetics, due to the timescales involved, that govern the initial stages of nucleation leading to film growth.

Ab initio calculations focusing on atomic diffusion on TM nitride surfaces are commonly used to determine minimum energy paths and corresponding diffusion barriers at 0 K [24–26]. Generally, this is accomplished by determining adspecies static adsorption-energy landscapes, or using algorithms such as the nudged elastic band (NEB) method [27,28]. However, the rate of thermally-activated migration events depends not only on diffusion barriers, but also on jump attempt frequencies [29]. Vineyard showed that the latter can be estimated within the harmonic approximation at 0 K from the ratio of the product of the N phonon frequencies at the starting point of the transition to the (N–1) phonon frequencies of the system constrained in the transition-state saddle-point configuration [30,31].

While providing estimates of diffusion barriers and attempt frequencies, the computational approaches described above do not account for

* Corresponding author. Tel.: +46 13282623; fax +46 13137568.
E-mail address: davsan@ifm.liu.se (D.G. Sangiovanni).

http://dx.doi.org/10.1016/j.susc.2014.04.007
0039-6028/

the fact that activation energies and pathways are affected by atomic vibrations at finite temperatures. Moreover, Arrhenius exponential prefactors estimated from 0 K phonon calculations do not accurately describe diffusion attempt-frequencies for materials characterized by large anharmonic contributions to atomic interactions. The approximation proposed by Vineyard [31] is not applicable to TM nitride compounds, such as B1 NaCl-structure vanadium nitride, which are predicted to be dynamically unstable at 0 K [32]. Molecular dynamics (MD) simulations are the most accurate and reliable approaches available to determine surface diffusion jump rates and pathways at finite temperatures.

In MD simulations, the atomic interactions can be described by first-principles or empirical formulations; both methods have advantages and disadvantages. Density functional theory (DFT) is, in principle, the most accurate methodology available to calculate interatomic forces during MD runs [33]. However, DFT has several limitations [34]. The approximations used in DFT for estimation of electron exchange and correlation energy are optimized to describe three-dimensional lattices. However, the abrupt changes which occur in the electron density at surfaces can result in under- or overestimation of surface/adsorbate bond strengths, and hence incorrect adsorption energies [35]. This, in turn, results in incorrect predictions for the relative stabilities of different adsorption sites [36] and, in DFT-based ab initio molecular dynamics (AIMD) simulations of surface kinetics, in incorrect predictions of preferred adsorbate diffusion pathways and jump rates.

Highly computationally demanding AIMD/DFT runs are also limited to the simulation of small systems (a few hundred atoms) and for short time intervals (a few nanoseconds). This does not allow investigation of the effects of phonon wavelength degrees of freedom on atomic migration, estimation of the effect of correlated jumps on diffusion coefficients, or obtaining well-converged values of rate constants for rare events. These limitations are easily overcome when, instead of DFT, empirical potentials are used for the description of interatomic forces. However, classical molecular dynamics (CMD) simulations based upon empirical potentials are less accurate than quantum-mechanical approaches. Despite their individual limitations, AIMD and CMD simulations can be used in parallel to provide complementary information. When AIMD and CMD results are consistent, it is reasonable to assume that the agreement is not accidental, and that the theoretical predictions are realistic representations of actual physical phenomena.

In this study, we probe the dynamics of Ti adatoms on TiN(001) as a function of temperature by performing both AIMD simulations based on DFT and CMD simulations in which the interatomic forces are obtained from the modified embedded atom method (MEAM) potential parameterized to reproduce TiN bulk, as well as surface, properties [37–39]. Titanium nitride, one of the first hard-coating materials [15,40,41], serves as a model to probe diffusion dynamics and kinetics on NaCl-structure TM nitride surfaces in general.

AIMD/DFT and CMD/MEAM simulations show that Ti adatoms on TiN(001) favor fourfold-hollow positions, surrounded by two Ti and two N surface atoms; adatom migration between these sites occurs primarily via in-plane <100> channels. We determine activation energies E_a and jump-attempt frequencies A of the most frequently observed Ti adatom diffusion pathways on TiN(001) extrapolated from jump-rate ln(k) vs. inverse temperature 1/T Arrhenius plots, in which k is the rate constant. We assess the effect of increasing phonon wavelength degrees of freedom by using progressively larger simulation supercells in CMD runs. Finally, the Ti adatom normal distributions on TiN(001), obtained using uncorrelated jump probabilities $Aexp[-E_a/(k_BT)]$, are employed to determine the surface diffusion coefficient D_s as a function of temperature T. The latter values are compared to those extracted directly from the adatom mean-square displacements during CMD runs to evaluate correlation between consecutive jumps. Remarkably, diffusion coefficient results obtained from AIMD and CMD are in good agreement at all temperatures.

2. Computational details

MD simulations are performed within the microcanonical ensemble NVE, while the substrate temperature is maintained constant via periodic rescaling of the atomic velocities, which mimics a canonical NVT sampling of configurational space [42]. Standard Verlet algorithms are used to integrate Newton's equations of motion at 1 fs time intervals for both CMD and AIMD runs. CMD simulations are carried out by describing atomic interactions with the second-neighbor MEAM [43] potential as implemented in the large-scale atomic/molecular massively parallel simulator (LAMMPS) [44]. We use the TiN MEAM parameters from our previous publications [37–39,45], which were shown to yield diffusion barriers, Ehrlich step-edge barriers, surface formation energies, step-edge formation energies, and adatom formation energies which are consistent with experimental values [18,20,46], as well as a description of single N adatom and N adatom pair interactions on TiN(001) which are in agreement with AIMD/DFT simulation predictions [39]. Ab initio molecular dynamics simulations are carried out with the VASP code [47] implemented using the generalized gradient approximation (GGA) [48] and the projector augmented wave (PAW) [49] method. The Brillouin zone is sampled with $3 \times 3 \times 1$ k-point grids centered at the Γ point. At each time step, the total energy is evaluated to an accuracy of 10^{-5} eV/atom using a plane-wave energy cutoff of 400 eV.

Ti adatom diffusion pathways and jump rates are probed as a function of temperature on 3×3 TiN(001) surface unit cells. The substrate consists of three layers for a total of 108 atoms in AIMD runs, and eight layers with 288 atoms in CMD runs. The lateral size of the simulation cell is sufficient to avoid adatom self-interactions. During all MD runs, the bottom slab layer remains fixed. This does not affect the substrate temperature, which depends only on the atomic-motion translational degrees of freedom. AIMD simulation boxes contain six vacuum layers to prevent interaction between TiN(001) surface slab replicas along the [001] direction. At each temperature, the average Ti–N in-plane nearest-neighbor distance $<d_{NN//}>$ in the simulation slab is obtained, accounting for the experimental TiN thermal expansion coefficient $9.35 \times 10^{-6}\ K^{-1}$ [4], by rescaling the 0 K $<d_{NN//}>$ values, 2.127 Å for DFT + GGA [50] and 2.121 Å for MEAM [37]. Rescaling of $<d_{NN//}>$ as a function of temperature is necessary to avoid spurious substrate strain effects on the adatom jump rate [51]. Prior to initiating each MD run, thermal oscillations in the adatom-free simulation slab are allowed to stabilize for 5 ps, a time interval sufficient to equilibrate the phonon modes in the system.

Ten statistically independent CMD runs of 10 ns are performed at temperatures T of 600, 900, 1200, and 1500 K for a total of 0.4 μs simulated time. 0.5-ns AIMD runs are performed at 1000, 1200, 1500, and 2200 K, for a total of 2 ns simulation time. All results are stored in video files with a time resolution of 10 fs. In order to further verify the reliability of our AIMD model, we vary the number of simulation slab layers from three to five (180 atoms) to test the dependence of the diffusion rate constant k on substrate thickness. Two 40-ps AIMD runs, performed at T = 2200 and 2500 K with the larger simulation cell, return jump-rates which are in good agreement with those calculated for three-layer slabs.

We use MEAM and DFT conjugate gradient minimizations to calculate Ti adatom adsorption energy landscapes on 4×4 atom static TiN(001) supercells consisting of five layers, by sampling the irreducible triangle of the surface unit cell on a 25-point grid. This is accomplished by relaxing the upper two TiN(001) layers and the vertical coordinates of the adspecies at each point. Adsorption energies are evaluated to an accuracy of 10^{-5} eV/atom, which in DFT is achieved by using a plane-wave cutoff of 500 eV and integrating the Brillouin zone on $15 \times 15 \times 1$ k-point meshes centered at Γ. Both quantum-mechanical and empirical results indicate that the most stable position for isolated Ti adatoms on infinite TiN(001) terraces at 0 K is in fourfold hollow sites surrounded by two Ti and two N surface atoms (Fig. 1). Considering the

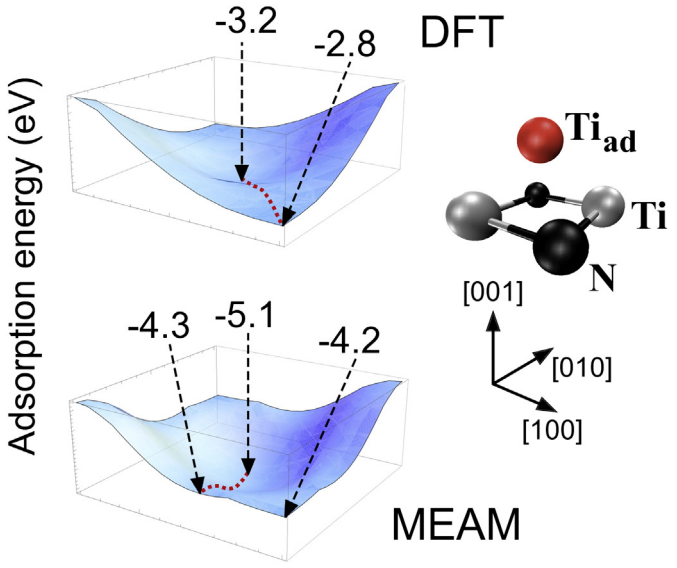

Fig. 1. Adsorption energy landscapes for Ti adatoms on a TiN(001) surface unit cell. A schematic view of the surface unit cell is shown to the right of the image. Adsorption energies are calculated with respect to the total energy of a Ti atom in the gas phase. Minimum energy paths connecting stable fourfold hollow sites, determined from the curvature of the potential energy surface, and confirmed by NEB calculations, are shown by the red dotted lines. Adsorption energies are indicated only for the most stable adsorption site (fourfold hollow), the metastable epitaxial site, and, in MEAM results, for the energetically-favored position at the surface unit cell boundary, a Ti–N bridge site closer to the N surface atom.

uncertainty regarding the accuracy of DFT for surface calculations [35,36,52], the agreement between DFT + GGA and MEAM predictions (see adsorption energy values in Fig. 1) for Ti monomer stability at various surface sites is quite good.

In order to determine the preferred adsorption position of Ti adatoms on TiN(001) at temperatures between 1000 and 2200 K, we perform preliminary AIMD tests in which the initial adatom (x, y) coordinates are randomly chosen at a distance of ~2 Å above the surface. In all cases, Ti adatoms quickly reach and remain in fourfold hollow sites, in accordance with the predictions of our present 0 K DFT and MEAM calculations, and previous CMD simulations at 1000 K [37]. Thus, a fourfold hollow site is chosen as the starting position for Ti adatoms in all MD runs.

For each Ti adatom diffusion pathway $m\left[\vec{r}_i \rightarrow \vec{r}_i + \vec{r}_j\right]$ (for simplicity, expressed as $m(i \rightarrow j)$) between neighboring i and j fourfold hollow sites on TiN(001) terraces, we determine activation energies E_a and attempt frequencies A by linear interpolation of the logarithm of the jump rate k(T) (obtained from MD runs as a function of T) vs. inverse temperature as prescribed by the Arrhenius equation:

$$\ln\left[k^{m(i\rightarrow j)}(T)\right] = \ln\left[A^{m(i\rightarrow j)}\right] - \frac{E_a^{m(i\rightarrow j)}}{k_B}\left(\frac{1}{T}\right). \quad (1)$$

The uncertainties σ_κ, σ_A, and σ_E, associated with the values of rate coefficient ln(k), attempt frequency A, and activation energy E_a, are estimated following the scheme reported in reference [39].

Ti adatom surface diffusion coefficients D_s on TiN(001) are determined from the normalized probability distribution function $P\left(\vec{r}, t, T\right)$, which corresponds to the probability of finding the adspecies in a (001) surface unit cell centered at position $\vec{r}$ at time t and temperature T, using the two-dimensional Einstein relation:

$$D_s(T) = \lim_{t\rightarrow\infty} \frac{\left\langle \left[\sum_{\vec{r}} P(\vec{r}, t, T)\cdot|\vec{r}|\right]^2 \right\rangle}{4t}. \quad (2)$$

The summation in Eq. (2) extends over all (001) surface lattice vectors $\vec{r}$, and P at time $t = 0$ is a Dirac delta function centered at the adatom initial position $\vec{r} = 0$. Eq. (2) yields diffusion coefficients corresponding to adatom random walks (uncorrelated jumps) on TiN(001).

$P\left(\vec{r}, t, T\right)$ can be calculated using transition probabilities from sites i to sites j: $A^{m(i\rightarrow j)}\exp[-E_a^{m(i\rightarrow j)}/(k_BT)]$. At any temperature T, P at time $(t + \Delta t)$ is obtained from P at time t plus an inward flux Φ_{in}, i.e. the probability for the adatom $m(i \rightarrow j)$ migration from neighboring surface unit cells into the fourfold hollow site at position $\vec{r}$, minus an outward transition probability Φ_{out} due to adspecies moving from position $\vec{r}$ to neighboring sites via $m(i \rightarrow j)$. Thus,

$$P\left(\vec{r}, t+\Delta t, T\right) = P\left(\vec{r}, t, T\right) + \Phi_{in} - \Phi_{out}, \quad (3)$$

for which

$$\Phi_{in} = \sum_{\vec{r}_j}\left\{P\left(\vec{r}+\vec{r}_j, t, T\right)A^{m(i\rightarrow j)}\exp\left[-E_a^{m(i\rightarrow j)}/(k_BT)\right]\Delta t\right\}, \quad (4)$$

and

$$\Phi_{out} = \sum_{\vec{r}_j}\left\{P\left(\vec{r}, t, T\right)A^{m(i\rightarrow j)}\exp\left[-E_a^{m(i\rightarrow j)}/(k_BT)\right]\Delta t\right\}. \quad (5)$$

The summations in Eqs. (4) and (5) extend over all $\vec{r}_j$ vectors connecting neighboring surface fourfold hollow sites to which the adatom can migrate via the diffusion mechanism $m(i \rightarrow j)$. The normalization of P is preserved at any given time t provided that the interval Δt is much smaller than the inverse jump rate $1/k$ at temperature T. The uncertainty $|\sigma_D(T)|$ associated with surface diffusion coefficients values $D_s(T)$ deriving from stochastic Ti adatom walks on TiN(001) is obtained from the relationship: $|\sigma_D(T)| = |D_{max}(T) - D_{min}(T)|/2$. Upper and lower boundary values, $D_{max}(T)$ and $D_{min}(T)$, of the diffusion coefficient are obtained from Eqs. (2) to (5) by applying the substitutions $[A \rightarrow A + \sigma_A/\sqrt{2};\ E_a \rightarrow E_a - \sigma_E/\sqrt{2}]$ and $[A \rightarrow A - \sigma_A/\sqrt{2};\ E_a \rightarrow E_a + \sigma_E/\sqrt{2}]$, respectively.

After a sufficiently long time $t \gg 1/k$, $P\left(\vec{r}, t, T\right)$ becomes a uniform radial distribution function $\overline{P}(r, t, T)$. Thus, at time t and temperature T, the normalized probability $\overline{P}(r, t, T)$ to find a Ti adatom at a distance r from its initial position is

$$\overline{P}(r, t, T) = \frac{P\left(\vec{r}, t, T\right)\times 2\pi r\Delta r}{\sum_r\left[P\left(\vec{r}, t, T\right)\times 2\pi r\Delta r\right]}, \quad (6)$$

and the average adatom displacement $\langle\alpha(t, T)\rangle$ can be obtained from:

$$\langle\alpha(t, T)\rangle = \sum_r\left[r\times\overline{P}(r, t, T)\Delta r\right] = \sqrt{4tD_s(T)}. \quad (7)$$

By linear interpolation of $\ln[D_s(T)]$ vs. $1/T$, we extract convolved values (since Ti adatom diffusion occurs via more than one pathway) of Arrhenius prefactors A′ and diffusion barriers E_a', which correspond to the radial (isotropic) diffusion of Ti adspecies on TiN(001) surfaces:

$$\ln[D_s(T)] = \ln(A') - \frac{E_a'}{k_B}\left(\frac{1}{T}\right). \quad (8)$$

The magnitude of $\sigma_D(T)$ affects those of the uncertainties σ_A' and σ_E', which are associated with the values of A′ and E_a', respectively. σ_A' and σ_E' are assessed by following the scheme described previously [39].

In CMD runs, we progressively enlarge the simulation slab, from 3×3 to 5×5, 8×8, 12×12, and 17×17 surface unit cells (for a total of 288, 800, 2048, 4608, and 9248 atoms, respectively), to investigate the effect on Ti adatom mobility of increasing the phonon wavelength degrees of freedom. We perform ten 10-ns CMD runs, at each of the temperatures

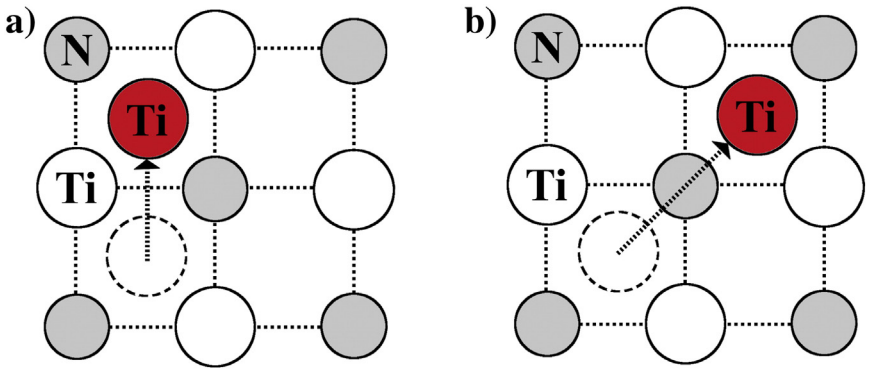

Fig. 2. Schematic representation of Ti adatom net translations on TiN(001) surfaces connecting stable fourfold hollow site positions as observed in AIMD and CMD videos. (a) In-plane <100> single jumps and (b) in-plane <110> single jumps crossing metastable epitaxial sites atop N surface atoms.

listed above for each supercell size, yielding a total simulated time of 2 μs, and find that a 17 × 17 unit cell surface area is sufficient to achieve saturation of calculated A′ and E_a' values.

Finally, $D_s(T)$ results obtained by multiplying uncorrelated transition probabilities (Eqs. (2)–(5)) are compared with $D_s^{corr}(T)$ values calculated from the two-dimensional Einstein relation:

$$D_s^{corr}(T) = \lim_{t\to\infty} \frac{\left\langle [\vec{r}(t) - \vec{r}(0)]^2 \right\rangle}{4t}, \quad (9)$$

for which adspecies mean-square displacements are tracked during 10-ns CMD simulations on large TiN(001) terraces (8 × 8, 12 × 12, and 17 × 17 surface unit cells), at the temperatures listed above, for a total of 120 runs. We also use data collected during our previous CMD investigations [37] of Ti adatom dynamics on 9 × 9 surface unit cell TiN(001) simulation slabs at 1000 K. The comparison between $D_s(T)$ and $D_s^{corr}(T)$ values allows us to estimate the effect of correlated jumps on the diffusion coefficient. At any given temperature, the uncertainty $\sigma_D^{corr}(T)$ associated with D_s^{corr} values is calculated via the relationship: $\sigma_D^{corr}(T) = [\ln(\overline{D}_s^{corr}(T)/D_{min}^{corr}(T)) + \ln(D_{max}^{corr}(T)/\overline{D}_s^{corr}(T))]/2$ [53], for which the average, $\overline{D}_s^{corr}(T)$, and the extreme, $D_{min}^{corr}(T)$ and $D_{max}^{corr}(T)$, values of the diffusion coefficient are determined from 30 CMD runs. D_s^{corr} values outside the range $[D_{min}^{corr}(T),\ D_{max}^{corr}(T)]$ are unlikely. Activation energies $E_a'^{corr} \pm \sigma_E'$ and exponential prefactors $A'^{corr} \pm \sigma_A'$, corresponding to correlated/isotropic Ti adatom surface diffusion, are obtained in analogy with uncorrelated isotropic values.

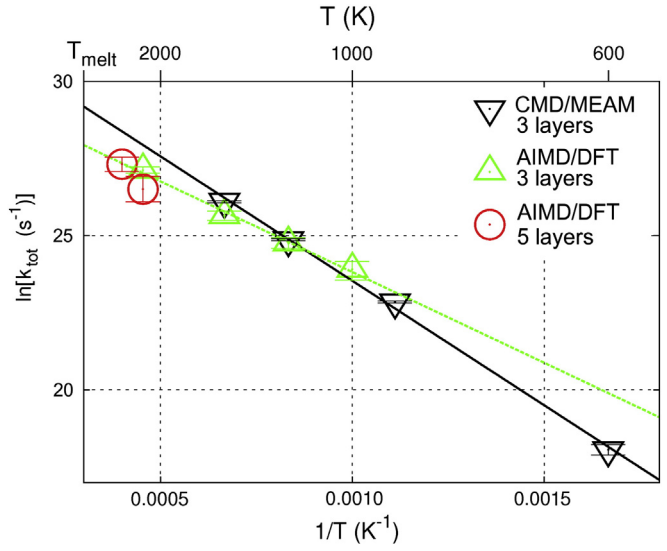

Fig. 3. Ti adatom total jump rate k_{tot}, obtained from AIMD and CMD simulations, vs. inverse temperature 1/T. $\ln(k_{tot})$ values obtained from AIMD runs on thicker simulation slabs comprised of five TiN(001) atomic layers are within the uncertainty range σ_κ of three-layer AIMD results. Error bars indicate uncertainties σ_κ (see Section 2). T_{melt} ~3000 °C is the melting point of TiN.

3. Results and discussion

MD movies show that in-plane <100> and <110> translations (Fig. 2), the latter passing atop a N surface atom, are the preferred diffusion pathways for Ti adatoms migrating between neighboring fourfold-hollow sites on TiN(001).

In CMD runs, Ti <100> migration is slightly bowed; the adatom passes closer to N than to Ti while crossing the boundary between nearest-neighbor surface unit cells. This is consistent with the curvature of the adsorption energy landscapes obtained from MEAM 0 K calculations (Fig. 1), which show that the Ti adatom minimum energy path connecting neighboring fourfold-hollow sites crosses the Ti–N surface-atom bond via a saddle point located nearer to N. The latter is due to the higher affinity of the Ti adatom for N than for Ti surface atoms. Ti adatom <110> jumps always occur with the adspecies passing atop metastable epitaxial sites, where they spend up to a few femtoseconds.

In AIMD simulations, Ti adatoms always transit through metastable epitaxial positions during migration on TiN(001). Once atop a N surface atom, where the adatom resides for a few fs, it can return to the initial stable site (resulting in no net migration), proceed along the same <110> direction, or move orthogonal to the initial motion, thus yielding a net <100> translation. This result is consistent with DFT 0 K adsorption energy landscapes (see Fig. 1 and references [24,25]), showing that the minimum energy path connecting neighboring fourfold hollow sites is across N atop positions.

Both CMD and AIMD runs reveal that Ti adatoms can also perform <100> and <110> double jumps on TiN(001) terraces. <100> double jumps are the second most frequently recorded diffusion mechanism during CMD runs. For this reason, double-jump attempt frequencies and activation energies are calculated separately. In AIMD runs, double jumps take place along <110> more often than along <100>. However, due to limited AIMD simulation times, it is not possible to determine accurate rate coefficients for long jumps, which are instead counted as multiple single-migration events.

Fig. 3 shows CMD and AIMD Arrhenius plots of the temperature dependent total jump rate k_{tot} of Ti adatoms migrating on TiN(001). To obtain k_{tot}, each double jump corresponds to two migration events. k_{tot} obtained from AIMD runs also includes diffusion events in which an adatom moves from a fourfold hollow site to an epitaxial site, and then returns to the initial position. Remarkably, CMD and AIMD simulations provide very similar diffusion rates. From the total number of migration events, we extract $E_a = (0.51 \pm 0.03)$ eV and $A = (0.79 \pm 0.14) \times 10^{13}\ s^{-1}$ for AIMD, and $E_a = (0.69 \pm 0.02)$ eV and $A = (5.30 \pm 0.80) \times 10^{13}\ s^{-1}$ for CMD. We note that the AIMD activation energy of 0.51 eV is almost 50% higher than that obtained from DFT/NEB calculations on static TiN(001) terraces of the same size [24]. A similar difference was

observed when comparing the barriers estimated from DFT/NEB and AIMD/DFT for N adatom diffusion on TiN(001) [39]. These results highlight the fact that lattice vibrations strongly affect the energetics of adatom diffusion on TiN(001).

Fig. 4a is a plot of Ti adatom jump rates as a function of T for the two migration pathways observed during AIMD runs, i.e. <100> and <110> single jumps. The AIMD simulations result in a linear Arrhenius ln(k) vs. 1/T behavior for both diffusion mechanisms. From the interpolation of ln(k) data points, using Eq. (1), we extract $E_a = (0.54 \pm 0.06)$ eV and $A = (0.53 \pm 0.22) \times 10^{13}\ s^{-1}$ for <100> single jumps and $E_a = (0.44 \pm 0.07)$ eV and $A = (0.15 \pm 0.08) \times 10^{13}\ s^{-1}$ for <110> jumps. The trends for ln(k) values vs. 1/T suggest that <100> jumps occur more frequently than <110> jumps for T>1000 K, while <110> migration becomes the most likely mechanism at T<1000 K. Nevertheless, since AIMD uncertainties $\sigma_\kappa(T)$ are large with respect to the difference between <100> and <110> diffusion rates (see error bars in Fig. 4a), it is not possible to provide accurate estimates of the relative occurrence probability of <100> and <110> hops as a function of temperature.

CMD simulations predict that <100> migration is the preferred Ti adatom pathway on TiN(001) at all temperatures. <100> single jumps are the most frequently observed diffusion events, followed by <100> double jumps, and <110> single jumps (see Fig. 4b); activation energies and attempt frequencies are $E_a = (0.66 \pm 0.03)$, (0.88 ± 0.04), and (0.95 ± 0.06) eV and $A = (2.80 \pm 0.80)$, (3.07 ± 1.05), and $(1.61 \pm 0.73) \times 10^{13}\ s^{-1}$, respectively. The ratio between the rates of <100> double and single jumps increases with T. Double jumps account for approximately 5% of the total number of <100> migration events at 900 K and 25% at 1500 K. During CMD simulations performed at 1200 and 1500 K, we also observe Ti adatom <100> triple jumps and <110> double jumps. These, however, account for only 0.1% of the total number of diffusion events. The fact that long jumps become statistically more relevant with increasing T is consistent with AIMD results, in which double jumps occur only at $T \geq 1500$ K, with the highest probability, approximately 20% of the total number of diffusion events, obtained during simulations performed at 2200 K.

In CMD runs performed at 1500 K, we also observe Ti adatom diffusion occurring by exchange with a Ti surface atom. The Ti adatom moves downward into the TiN(001) substrate with a frequency of approximately 30 events per μs. The strain induced in the lattice by the migration of an interstitial Ti atom propagates horizontally within the (001) plane until one of the Ti atoms in the outermost slab layer moves upward onto the surface, thus becoming an adatom. However, this pathway is not observed in our AIMD simulations due to the very low occurrence frequency.

AIMD simulations are confined, because of the high computational cost, to the study of relatively small supercells. This limits the possibility of probing the effect of long wavelength phonons on adatom mobility. However, such effects can be studied in CMD runs. Fig. 5 shows the Arrhenius plots of total jump rates vs. 1/T recorded during CMD simulations of Ti adatoms migrating on TiN(001) eight-layer supercells with progressively increasing lateral sizes: 3 × 3, 5 × 5, 8 × 8, 12 × 12, and 17 × 17 surface unit cells. While k_{tot} increases significantly (by a factor of 2.5) with supercell area at 600 K, its percentage variation is negligible at higher temperatures. Thus, long-wavelength lattice vibrations promote significantly adsorbate mobility only at lower temperatures.

The insets in Fig. 5 are plots of CMD-calculated activation energies E_a and attempt frequencies A, corresponding to the total number of diffusion events, as a function of the supercell surface area. E_a and A reach asymptotic values of (0.62 ± 0.01) eV and $(2.76 \pm 0.23) \times 10^{13}\ s^{-1}$ for the largest of the supercells (17 × 17 surface unit cells). We note that the same E_a and A values would be obtained for small supercells (3 × 3 surface unit cells) by linear interpolation of the CMD Ti adatom

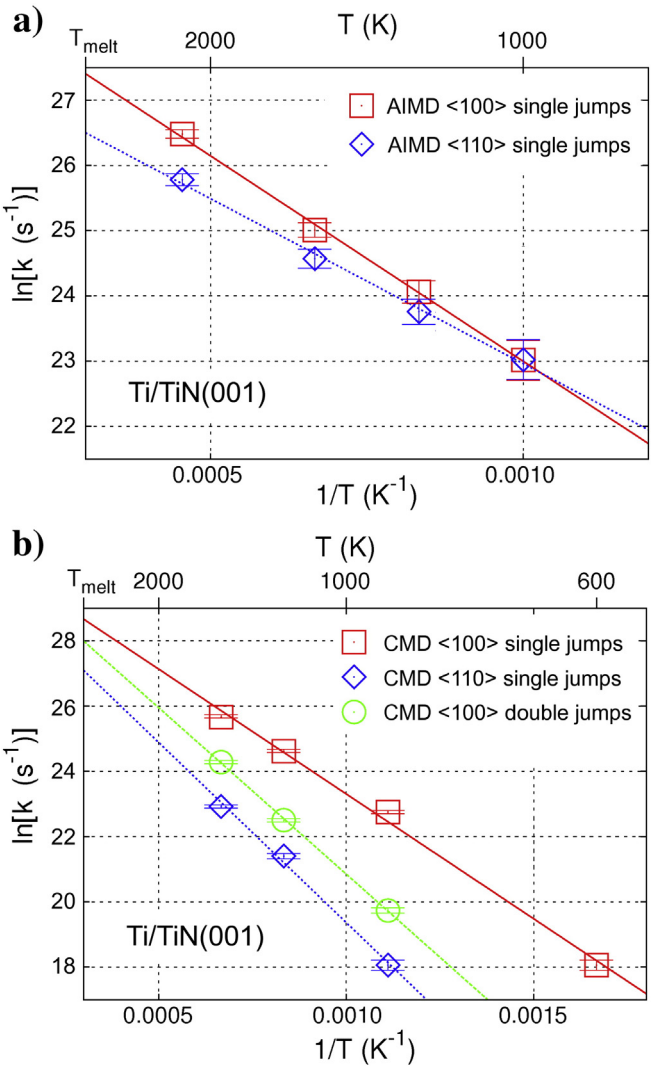

Fig. 4. Ti adatom jump rate ln(k) vs. inverse temperature 1/T for the primary diffusion pathways on TiN(001). (a) AIMD simulation results and (b) CMD simulation results. Error bars indicate uncertainties σ_κ (see Section 2).

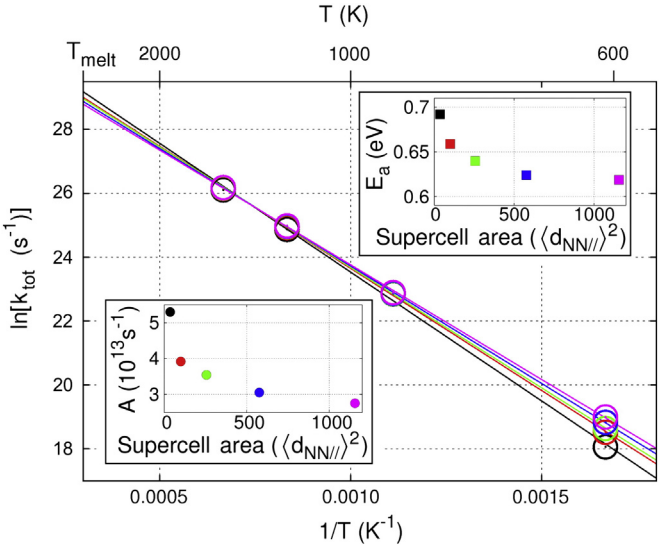

Fig. 5. Ti adatom total jump rate k_{tot}, obtained from CMD simulations, vs. inverse temperature 1/T. The TiN(001) supercell area is increased from 3 × 3 (black) to 5 × 5 (red), 8 × 8 (green), 12 × 12 (blue), and 17 × 17 (purple) surface unit cells. The insets show diffusion activation energy and attempt frequency dependence on the TiN(001) supercell area. (For interpretation of the references to color in this figure legend, the reader is referred to the web version of this article.)

Table 1
AIMD and CMD activation energies E_a and prefactors A, calculated using Eq. (1), for preferred Ti adatom diffusion pathways on TiN(001).

Ti/TiN(001)	AIMD		CMD	
	E_a (eV)	A (10^{13} s^{-1})	E_a (eV)	A (10^{13} s^{-1})
All jumps	0.51 ± 0.03	0.79 ± 0.14	0.62 ± 0.01	2.76 ± 0.23
Single <100>	0.54 ± 0.06	0.53 ± 0.22	0.57 ± 0.01	1.09 ± 0.10
Single <110>	0.44 ± 0.07	0.15 ± 0.08	0.81 ± 0.03	0.51 ± 0.14
Double <100>	–	–	0.84 ± 0.01	3.36 ± 0.15

total jump rates at temperatures ≥ 900 K. Thus, at high T, the number of diffusion events per unit time converges rapidly with supercell size. This suggests that the AIMD jump rate values shown in Figs. 3 and 4a, with a corresponding activation energy $E_a = (0.51 \pm 0.03)$ eV and attempt frequency $A = (0.79 \pm 0.14) \times 10^{13}$ s^{-1}, are saturated with respect to supercell surface area.

The higher phonon-mode degrees of freedom, achieved by increasing the surface area from 3 × 3 to 17 × 17 unit cells, affects the occurrence probability of all diffusion pathways. Ti adatom <100> single jumps are still the most frequently recorded events. <100> jump activation energies and attempt frequencies calculated for small supercells, $E_a^{3\times3} = (0.66 \pm 0.03)$ eV and $A^{3\times3} = (2.80 \pm 0.80) \times 10^{13}$ s^{-1}, both decrease for large simulation slabs; $E_a^{17\times17} = (0.57 \pm 0.01)$ eV and $A^{17\times17} = (1.09 \pm 0.10) \times 10^{13}$ s^{-1}. At 600 K, <100> single-jump rates increase by a factor of 2.6, while a slight decrease of 12% is observed at 1500 K because of the increasingly significant fraction of long jumps. Due to lattice vibrations with larger wavelength, the <100> double-jump activation energy decreases from $E_a^{3\times3} = (0.88 \pm 0.04)$ eV to $E_a^{17\times17} = (0.84 \pm 0.01)$ eV, while the corresponding attempt frequency increases from $A^{3\times3} = (3.07 \pm 1.05) \times 10^{13}$ s^{-1} to $A^{17\times17} = (3.36 \pm 0.15) \times 10^{13}$ s^{-1}. Overall, the occurrence of double jumps increases at all temperatures. Ti adatom <100> double jumps are never observed during 0.1 μs CMD movies at 600 K. However, the jump rate estimated at 900 K for small supercells, $k^{3\times3} = (3.7 \pm 0.2) \times 10^8$ s^{-1}, increases by 80% for large simulation substrates, $k^{17\times17} = (6.6 \pm 0.1) \times 10^8$ s^{-1}, and by 45% at 1500 K: $k^{3\times3} = (3.5 \pm \varepsilon) \times 10^{10}$ s^{-1} and $k^{17\times17} = (5.1 \pm \varepsilon) \times 10^{10}$ s^{-1}, in which $\varepsilon \ll 0.1$.

As was the case for 3 × 3 surface unit cells, <110> single jumps are the least frequently observed diffusion mechanisms for 17 × 17 unit cells. Nevertheless, <110> jump rates increase significantly on large supercells; the corresponding activation energy and attempt frequency range from $E_a^{3\times3} = (0.95 \pm 0.06)$ eV and $A^{3\times3} = (1.61 \pm 0.73) \times 10^{13}$ s^{-1} to $E_a^{17\times17} = (0.81 \pm 0.03)$ eV and $A^{17\times17} = (0.51 \pm 0.14) \times 10^{13}$ s^{-1}. AIMD and CMD estimates of diffusion barriers E_a and jump attempt frequencies A for the three primary Ti adatom pathways on TiN(001) are summarized in Table 1. We note that uncertainties σ_A and σ_E are considerably reduced upon increasing the supercell size, as diffusion rates $\ln(k^{17\times17})$ vary with 1/T in a more linear fashion than for 3 × 3 supercells. At 900 K, $k^{17\times17}$ is 2× larger than $k^{3\times3}$; the difference decreases to ~5% larger at 1500 K. The vibrational degrees of freedom for 34 × 34 atom TiN(001) simulation layers yield saturated values of Ti adatom total jump rates, which are higher than those recorded on small supercells by 160% at 600 K ($k_{tot}^{3\times3} = (0.7 \pm 0.2) \times 10^8$ s^{-1} and $k_{tot}^{17\times17} = (1.8 \pm 0.2) \times 10^8$ s^{-1}), and by 7% at 1500 K ($k_{tot}^{3\times3} = (21.8 \pm \varepsilon) \times 10^{10}$ s^{-1} and $k_{tot}^{17\times17} = (23.4 \pm \varepsilon) \times 10^{10}$ s^{-1}, where $\varepsilon \ll 0.1$).

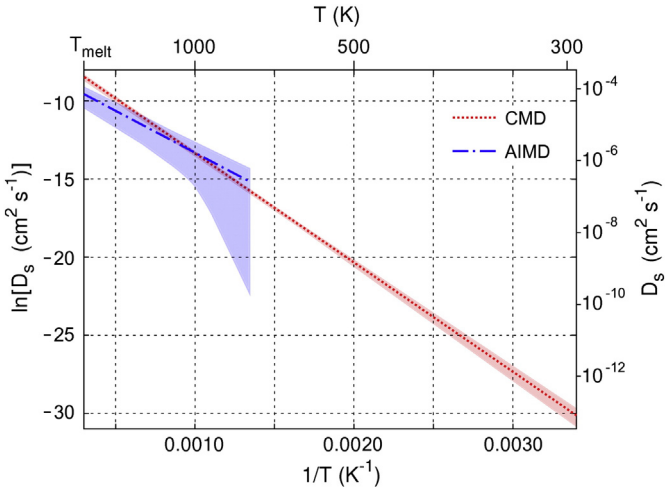

Fig. 6. CMD and AIMD Ti adatom diffusion coefficient D_s vs. inverse temperature 1/T for uncorrelated transition probabilities. Shaded regions correspond to uncertainties σ_D (see Section 2 and Table 2).

Table 2
Ti/TiN(001) adatom diffusion coefficient $D_s(T)$ obtained from CMD and AIMD simulations as a function of temperature T for correlated and uncorrelated events.

T (K)	D_s (cm^2 s^{-1})		
	Correlated	Uncorrelated	
	CMD	CMD	AIMD
300	–	$(1.3 \pm 0.6) \times 10^{-13}$	$\sigma_D > D$
600	$(1.0 \pm 0.7) \times 10^{-8}$	$(1.5 \pm 0.2) \times 10^{-8}$	$\sigma_D > D$
900	$(5.0 \pm 2.1) \times 10^{-7}$	$(7.3 \pm 0.9) \times 10^{-7}$	$(9.2 \pm 8.9) \times 10^{-7}$
1000	[a] $(5.2 \pm 1.9) \times 10^{-7}$	$(1.6 \pm 0.2) \times 10^{-6}$	$(1.7 \pm 1.5) \times 10^{-6}$
1200	$(3.9 \pm 1.4) \times 10^{-6}$	$(5.1 \pm 0.6) \times 10^{-6}$	$(4.1 \pm 3.2) \times 10^{-6}$
1500	$(0.5 \pm 0.2) \times 10^{-5}$	$(1.6 \pm 0.3) \times 10^{-5}$	$(1.0 \pm 0.7) \times 10^{-5}$
1800	–	$(3.6 \pm 0.5) \times 10^{-5}$	$(1.8 \pm 1.2) \times 10^{-5}$

[a] From reference [37].

Diffusion coefficients, which provide a well-defined measure of atomic mobility, depend upon both jump activation energies and attempt frequencies. Nevertheless, theoretical studies of atomic diffusion generally focus only on determination of diffusion barriers [24–26,54]. Using Eqs. (2)–(5), parameterized with the saturated values of activation energies and attempt frequencies obtained from AIMD and CMD jump rates for the different diffusion pathways, Ti adatom diffusion coefficients D_s on TiN(001) are evaluated as a function of temperature (see Fig. 6). Regardless of the fact that ab initio and classical methods predict different Ti adatom <100> and <110> jump rates, AIMD and CMD diffusion coefficients based purely on uncorrelated hops (random walk) are in good agreement over the investigated temperature range (see Fig. 6 and Table 2).

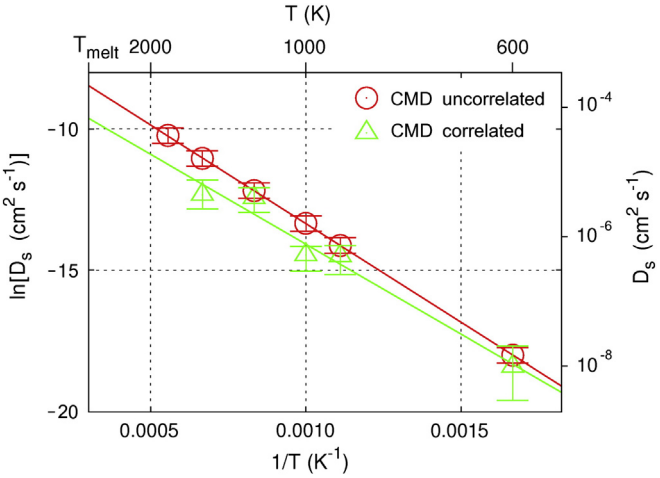

Fig. 7. Ti adatom diffusion coefficient D_s vs. inverse temperature 1/T obtained from CMD results. Open red circles (green triangles) correspond to diffusion coefficients determined from uncorrelated (correlated) Ti adatom transition probabilities between stable sites on TiN(001). Error bars indicate uncertainties σ_D (see Section 2). (For interpretation of the references to color in this figure legend, the reader is referred to the web version of this article.)

Table 3
AIMD and CMD convolved activation energies E_a' and attempt frequencies A' corresponding to Ti adatom ideal isotropic diffusion on TiN(001) as determined by AIMD and CMD.

Ti/TiN(001)	Correlated		Uncorrelated			
	CMD		CMD		AIMD	
	$E_a'^{corr}$ (eV)	A'^{corr} (10^{-4} cm^2 s^{-1})	E_a' (eV)	A' (10^{-4} cm^2 s^{-1})	E_a' (eV)	A' (10^{-4} cm^2 s^{-1})
Radially isotropic diffusion	0.55 ± 0.10	4.5 ± 3.2	0.60 ± 0.02	17.2 ± 3.8	0.46 ± 0.23	3.5 ± 2.8

An accurate evaluation of the Ti adatom mobility at temperatures ≤900 K is presently beyond the ability of AIMD/DFT simulations (see Table 2 and Fig. 6). The number of diffusion events recorded during AIMD runs is too low and produces uncertainties σ_D that exceed the magnitude of $D_s(T)$ values obtained from Eqs. (2) to (5). At T ≥ 900 K, AIMD D_s values are defined within a reasonably small uncertainty range, and confirm the reliability of the CMD estimations. This lends confidence that CMD-based D_s results are also reliable at T < 900 K. The uncertainties σ_D associated with the CMD results are relatively small considering that measured bulk TiN self-diffusion coefficients values range over three to four orders of magnitude [14,16,17].

Ti adatom distribution probabilities $P\left(\vec{r}, t, T\right)$ on TiN(001) are two-dimensional Gaussian functions provided that the time t in Eqs. (2)–(5) is much larger than the inverse jump rate at a given temperature. Thus, a linear interpolation of $\ln[D_s(T)]$ vs. 1/T (Eq. (8)) yields values for activation energy and attempt frequency which correspond to ideal radially isotropic Ti adatom diffusion on TiN(001) terraces. From AIMD calculations, $E_a' = (0.46 \pm 0.23)$ eV and $A' = (3.5 \pm 2.8) \times 10^{-4}$ cm^2 s^{-1}; for CMD $E_a' = (0.60 \pm 0.02)$ eV and $A' = (17.2 \pm 3.8) \times 10^{-4}$ cm^2 s^{-1}. $D_s(T)$ values are obtained from the relationship $D_s(T) = A' \exp[-E_a' / (k_B T)]$.

Determining diffusion coefficients from probability distribution functions, Eqs. (2)–(5), implicitly assumes that adatom jumps are completely uncorrelated. This, however, may not be the case. For example, when the rate of long jumps is significant (such as observed experimentally for W and Pd on W(110) and W(211) surfaces [55,56]), approximating atomic displacement distribution probabilities by counting a double-jump as two uncorrelated single jumps leads to an incorrect prediction of mass transport as a function of time. This occurs because a double-jump actually corresponds to two consecutive highly-correlated single jumps occurring along the same diffusion path. To probe the effect of correlated jumps on the Ti adatom diffusion coefficient, we calculate D_s^{corr} from Eq. (9) by directly tracking the adatom mean-square displacement on large TiN(001) simulation supercells during 10-ns CMD runs (see Section 2). Due to insufficient simulation time, correlated diffusion coefficients D_s^{corr} do not exhibit a perfectly linear Arrhenius behavior (see Fig. 7). However, D_s^{corr} values are lower than uncorrelated CMD D_s values at all temperatures, indicating that, because of correlation effects, the actual Ti adatom diffusion coefficients are smaller than those based purely on random walks. By linearly interpolating the $\ln(D_s^{corr}(T))$ data set vs. 1/T, we extract effective jump activation energies and attempt frequencies $E_a'^{corr} = (0.55 \pm 0.10)$ eV and $A'^{corr} = (4.5 \pm 3.2) \times 10^{-4}$ cm^2 s^{-1}.

Due to the short simulation times in AIMD, it is not possible to probe the effect of correlated adatom hops on diffusion coefficients. As noted at the beginning of this section, because of the low frequency of double jumps in AIMD runs, each of these events is counted as two single jumps. This approximation inevitably yields underestimated AIMD D_s values, as the atomic-displacement Gaussian probability distribution generated by the random walk of an adspecies performing N hops, in which N is a large integer number, of length L is narrower than that obtained from stochastically oriented N/n jumps (n is an integer) of length n × L. This error will be larger for higher k_{double}/k_{single} jump-rate ratios. Thus, for Ti adatom diffusion coefficients obtained from AIMD adatom-probability distributions, the error introduced in D_s by counting each double-jump as two single-jumps, partially cancels out the error caused by neglecting correlation effects between consecutive jumps. Accounting for the different limitations of the techniques used to determine surface diffusivity, the most reliable estimates of convolved diffusion barriers E_a' and jump attempt frequencies A' for Ti adatom radially isotropic diffusion on TiN(001) are summarized in Table 3. Remarkably, AIMD E_a' and A' values are close to $E_a'^{corr}$ and A'^{corr} values obtained from CMD.

Using CMD-calculated D_s and D_s^{corr} values in Eq. (7), we determine the dependence of the Ti adatom average displacement $<\alpha>$ on temperature T and time t (see Fig. 8). $<\alpha>$ obtained from CMD results is always within the uncertainty range of those obtained from AIMD.

4. Conclusions

AIMD/DFT and CMD/MEAM simulations reveal that Ti adatoms on TiN(001) reside in fourfold hollow positions, surrounded by two Ti and two N surface atoms, and that the preferred migration path between these sites is along in-plane <100> channels. Activation energies E_a and prefactors A for each of the three primary diffusion pathways are extracted from their jump-rate dependences on temperature. Uncorrelated jump probabilities $A\exp[-E_a / (k_B T)]$ are used to determine diffusion coefficients D_s which quantify the mobility of adatoms following purely random trajectories on the terrace. AIMD D_s results are consistent with CMD, and thus validate the predictions of our MEAM

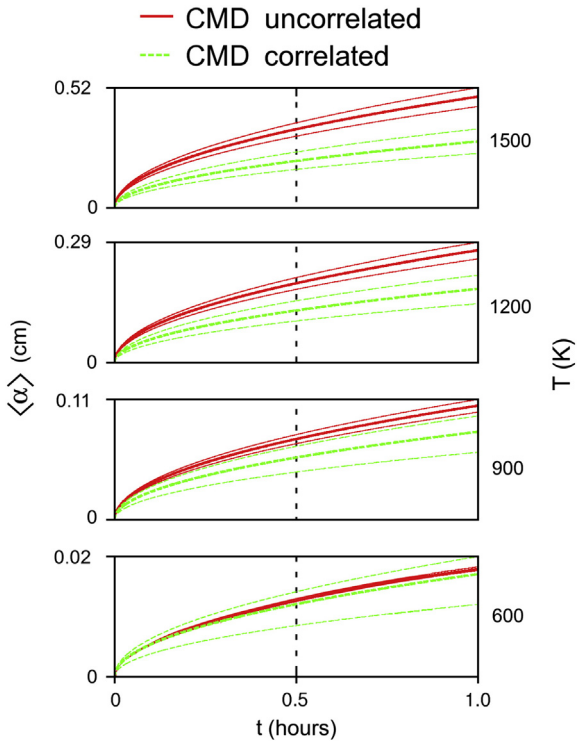

Fig. 8. Ti adatom average displacement $<\alpha>$ (thick lines), obtained from Eq. (7) parameterized with CMD diffusion coefficients deriving from correlated (green dashed lines) and uncorrelated (solid red lines) jumps, as a function of temperature T and time t. Thin lines define uncertainty ranges $[D_s(T) \pm \sigma_D(T)]$.

parameterization. CMD simulations are employed to probe the effect of increasing supercell areas (phonon wavelength degrees of freedom) on adatom hop rates and D_s. Finally, by directly tracking adspecies mean-square displacements during CMD runs, we observe that actual adatom diffusivities $D_s^{corr}(T)$, inherently accounting for correlation effects between consecutive jumps, are smaller than $D_s(T)$ at all temperatures.

Acknowledgments

Calculations were performed using the resources provided by the Swedish National Infrastructure for Computing (SNIC), on the Triolith Cluster located at the National Supercomputer Centre (NSC) in Linköping and on the Akka and Abisko clusters located at the High Performance Computing Center North (HPC2N) in Umeå, Sweden. We gratefully acknowledge financial support from the Knut and Alice Wallenberg Foundation (isotope project, 2011.0094), the Swedish Research Council (VR) Linköping Linnaeus Initiative LiLi-NFM (grant 2008-6572), and the Swedish Government Strategic Research Area Grant in Materials Science on Advanced Functional Materials (grant MatLiU 2009-00971).

References

[1] T. Reeswinkel, D.G. Sangiovanni, V. Chirita, L. Hultman, J.M. Schneider, Surf. Coat. Technol. 205 (2011) 4821.
[2] H. Kindlund, D.G. Sangiovanni, J. Lu, J. Jensen, V. Chirita, I. Petrov, J.E. Greene, L. Hultman, J. Vac. Sci. Technol. A 32 (2014) 030603.
[3] H. Kindlund, D.G. Sangiovanni, L. Martínez-de-Olcoz, J. Lu, J. Jensen, J. Birch, I. Petrov, J.E. Greene, V. Chirita, L. Hultman, Appl. Phys. Lett. Mater. 1 (2013) 042104.
[4] L.E. Toth, Transition Metal Carbides and Nitrides, Academic Press, New York, 1971.
[5] J.M. Molarius, A.S. Korhonen, E. Harju, R. Lappalainen, Surf. Coat. Technol. 33 (1987) 117.
[6] V.R. Parameswaran, J.P. Immarigeon, D. Nagy, Surf. Coat. Technol. 52 (1992) 251.
[7] M.A. Nicolet, Thin Solid Films 52 (1978) 415.
[8] I. Petrov, E. Mojab, F. Adibi, J.E. Greene, L. Hultman, J.E. Sundgren, J. Vac. Sci. Technol. A 11 (1993) 11.
[9] J.S. Chun, I. Petrov, J.E. Greene, J. Appl. Phys. 86 (1999) 3633.
[10] J.S. Chun, P. Desjardins, I. Petrov, J.E. Greene, C. Lavoie, C. Cabral, Thin Solid Films 391 (2001) 69.
[11] J.S. Chun, P. Desjardins, C. Lavoie, C.S. Shin, C. Cabral, I. Petrov, J.E. Greene, J. Appl. Phys. 89 (2001) 7841.
[12] H. Matzke, Diffusion in Carbides and Nitrides, Kluwer Academic Publ, Dordrecht, 1990.
[13] H. Matzke, Philos. Mag. 64 (1991) 1181.
[14] L. Hultman, Vacuum 57 (2000) 1.
[15] J.E. Sundgren, Thin Solid Films 128 (1985) 21.
[16] F.W. Wood, O.G. Paasche, Thin Solid Films 40 (1977) 131.
[17] F. Anglezioabautret, B. Pellissier, M. Miloche, P. Eveno, J. Eur. Ceram. Soc. 8 (1991) 299.
[18] S. Kodambaka, V. Petrova, A. Vailionis, P. Desjardins, D.G. Cahill, I. Petrov, J.E. Greene, Surf. Rev. Lett. 7 (2000) 589.
[19] S. Kodambaka, V. Petrova, A. Vailionis, P. Desjardins, D.G. Cahill, I. Petrov, J.E. Greene, Thin Solid Films 392 (2001) 164.
[20] S. Kodambaka, V. Petrova, A. Vailionis, I. Petrov, J.E. Greene, Surf. Sci. 526 (2003) 85.
[21] F. Watanabe, S. Kodambaka, W. Swiech, J.E. Greene, D.G. Cahill, Surf. Sci. 572 (2004) 425.
[22] S. Kodambaka, N. Israeli, J. Bareno, W. Swiech, K. Ohmori, I. Petrov, J.E. Greene, Surf. Sci. 560 (2004) 53.
[23] J. Bareno, S. Kodambaka, S.V. Khare, W. Swiech, V. Petrova, I. Petrov, J.E. Greene, TiN Surface Dynamics: Role of Surface and Bulk Mass Transport Processes, Mexico City, Mexico, 2006. 205.
[24] D. Gall, S. Kodambaka, M.A. Wall, I. Petrov, J.E. Greene, J. Appl. Phys. 93 (2003) 9086.
[25] B. Alling, P. Steneteg, C. Tholander, F. Tasnadi, I. Petrov, J.E. Greene, L. Hultman, Phys. Rev. B 85 (2012) 245422.
[26] Y. Ren, X.J. Liu, X. Tan, E. Westkamper, Comput. Mater. Sci. 77 (2013) 102.
[27] G. Henkelman, B.P. Uberuaga, H. Jonsson, J. Chem. Phys. 113 (2000) 9901.
[28] G. Henkelman, H. Jonsson, J. Chem. Phys. 113 (2000) 9978.
[29] D.G. Truhlar, B.C. Garrett, S.J. Klippenstein, J. Phys. Chem. 100 (1996) 12771.
[30] C. Wert, C. Zener, Phys. Rev. 76 (1949) 1169.
[31] G.H. Vineyard, J. Phys. Chem. Solids 3 (1957) 121.
[32] E.I. Isaev, S.I. Simak, I.A. Abrikosov, R. Ahuja, Y.K. Vekilov, M.I. Katsnelson, A.I. Lichtenstein, B. Johansson, J. Appl. Phys. 101 (2007) 123519.
[33] R. Car, M. Parrinello, Phys. Rev. Lett. 55 (1985) 2471.
[34] A.V. Ruban, I.A. Abrikosov, Rep. Prog. Phys. 71 (2008) 046501.
[35] L. Schimka, J. Harl, A. Stroppa, A. Gruneis, M. Marsman, F. Mittendorfer, G. Kresse, Nat. Mater. 9 (2010) 741.
[36] P.J. Feibelman, B. Hammer, J.K. Norskov, F. Wagner, M. Scheffler, R. Stumpf, R. Watwe, J. Dumesic, J. Phys. Chem. B 105 (2001) 4018.
[37] D.G. Sangiovanni, D. Edström, L. Hultman, V. Chirita, I. Petrov, J.E. Greene, Phys. Rev. B 86 (2012) 155443.
[38] D. Edström, D.G. Sangiovanni, L. Hultman, V. Chirita, I. Petrov, J.E. Greene, Thin Solid Films 558 (2014) 37.
[39] D.G. Sangiovanni, D. Edström, L. Hultman, I. Petrov, J.E. Greene, V. Chirita, Surf. Sci. 624 (2014) 25.
[40] H. Ljungcrantz, M. Oden, L. Hultman, J.E. Greene, J.E. Sundgren, J. Appl. Phys. 80 (1996) 6725.
[41] J.E. Greene, J.E. Sundgren, L. Hultman, I. Petrov, D.B. Bergstrom, Appl. Phys. Lett. 67 (1995) 2928.
[42] M.P. Allen, D.J. Tildesley, Computer Simulation of Liquids, Oxford University Press, 1989.
[43] B.J. Lee, M.I. Baskes, Phys. Rev. B 62 (2000) 8564.
[44] S. Plimpton, J. Comput. Phys. 117 (1995) 1.
[45] In our CMD simulations, we use a LAMMPS ialloy parameter value = 0, and ibar parameter value = 3. In Ref. [Y.M. Kim, B.J. Lee, Acta Mater. 56 (2008) 3481], ialloy = 2, ibar = 3.
[46] M.A. Wall, D.G. Cahill, I. Petrov, D. Gall, J.E. Greene, Surf. Sci. 581 (2005) L122.
[47] G. Kresse, J. Hafner, Phys. Rev. B 47 (1993) 558.
[48] J.P. Perdew, K. Burke, Y. Wang, Phys. Rev. B 54 (1996) 16533.
[49] P.E. Blöchl, Phys. Rev. B 50 (1994) 17953.
[50] D.G. Sangiovanni, V. Chirita, L. Hultman, Phys. Rev. B 81 (2010) 104107.
[51] H. Brune, K. Bromann, H. Roder, K. Kern, J. Jacobsen, P. Stoltze, K. Jacobsen, J. Norskov, Phys. Rev. B 52 (1995) 14380.
[52] M. Marlo, V. Milman, Phys. Rev. B 62 (2000) 2899.
[53] T. Nagy, T. Turanyi, In. J. Chem. Kinet. 43 (2011) 359.
[54] L. Tsetseris, N. Kalfagiannis, S. Logothetidis, S.T. Pantelides, Phys. Rev. Lett. 99 (2007) 4.
[55] D.C. Senft, G. Ehrlich, Phys. Rev. Lett. 74 (1995) 294.
[56] G. Antczak, G. Ehrlich, Phys. Rev. Lett. 92 (2004) 166105.